Minority-carrier lifetime and photoresponse properties of B-doped p-$BaSi_2$, a potential light absorber for solar cells

M. Emha Bayu[1], Cham Thi Trinh[2†], Ryota Takabe[1], Suguru Yachi[1], Kaoru Toko[1], Noritaka Usami[2], and Takashi Suemasu[1*]

[1]*Institute of Applied Physics, University of Tsukuba, Tsukuba, Ibaraki 305-8573, Japan*

[2]*Graduate School of Engineering, Nagoya University, Nagoya 464-8603, Japan*

†*Present address: Institut Silizium-Photovoltaik, Helmholtz-Zentrum Berlin für Materialien und Energie, Berlin 12489, Germany*

*E-mail: suemasu@bk.tsukuba.ac.jp

600-nm-thick B-doped p-$BaSi_2$ layers were grown on (111)-oriented n-Si substrates by molecular beam epitaxy, and the dependences of the minority carrier lifetime τ and photoresponsivity on the hole concentration p were investigated. p was varied from 1.4×10^{16} to 3.9×10^{18} cm^{-3}. The highest τ of 2 μs was obtained for the sample with the lowest p of 1.4×10^{16} cm^{-3}, reaching two orders of magnitude higher than that of the sample with the highest p of 3.9×10^{18} cm^{-3}. The low-concentration-doped sample also exhibited an excellent external quantum efficiency (*EQE*) as large as 80% at a wavelength of approximately 800 nm at a reverse bias voltage of 0.2 V. This value is higher than any other *EQE*s we have ever achieved for $BaSi_2$, showing the great potential of p-$BaSi_2$ as a light absorber in solar cells.

1. Introduction

Renewable energy resources play a critical role in coping with the huge energy demand due to the growing population and extensive usage of ever-growing electricity-consuming devices. Among such resources, solar cells are regarded as one of the best solutions. Today, more than 90% of installed solar cells are based on crystalline Si (c-Si) because of its abundance and advanced industrial technology.[1)] However, the performance of c-Si solar cells is limited by its bandgap E_g of 1.1 eV, which is narrower than the ideal E_g of approximately 1.4 eV for single-junction solar cells. Furthermore, owing to its small absorption coefficient, we need to employ at least 100-μm-thick layers to sufficiently absorb incoming photons, which is unfavorable for cost reduction.[2)] Many attempts have been employed to improve the energy conversion efficiency η, including structure engineering to establish an advanced light-trapping system in thin-film Si solar cells.[3-15)] However it is still difficult to obtain an η of 20%. Panasonic announced a record η of 25.6% realized by using a back-contact heterojunction with intrinsic thin-layer (HIT) solar cells[16)] surpassing the previous 24.7% record of front-emitter HIT cells.[17)] Many studies have also been conducted on various materials, such as chalcopyrite and cadmium telluride to realize higher η and lower cost.[18-23)] The pursuit of excellent alternative materials for solar cells is still ongoing. Among such materials, we have focused on semiconducting $BaSi_2$. The experimental results of optical absorption edge and photoresponsivity measurement show that $BaSi_2$ has an indirect bandgap of 1.3 eV, matching the solar spectrum.[24-29)] This result is also consistent with recent first-principles calculation using the Heyd-Scuseria-Ernzerhof screened hybrid functional published elsewhere.[30)] One of the key features of $BaSi_2$ is its large absorption coefficient α exceeding 3×10^4 cm^{-1} at photon energies higher than 1.5 eV in spite of its indirect bandgap.[27,31)] The diffusion length of minority carriers L in intrinsically doped n-$BaSi_2$ was found to be approximately 10 μm by an electron-beam-induced current technique, which is longer than its grain size of approximately 0.2 μm.[32)] Undoped $BaSi_2$ shows intrinsically n-type conductivity, with an electron concentration n on the order of 10^{16} cm^{-3}.[25)] A supercell approach based on first-principles density functional theory revealed that this n-type conductivity arises from Si vacancies.[33)] Hereafter, we denote intrinsically doped n-$BaSi_2$ simply as n-$BaSi_2$. The high α and large L of $BaSi_2$ suggest that $BaSi_2$ is suitable for thin-film solar cells; $\eta > 25\%$ can be expected in a 2-μm-thick $BaSi_2$ homojunction solar cell.[34)] Furthermore, $BaSi_2$ is composed of abundant Si and Ba; Si is the 2nd most abundant element, and Ba is the 16th most abundant element in the earth's crust.

A classic solar cell uses a pn junction. Thus, control of the conductivity of $BaSi_2$ by

impurity doping is required. The electrical properties of impurity (Cu, Ag, Sb, P, As, In, Al, or B)-doped $BaSi_2$ have been investigated.[35-43] Using an approach to realize $BaSi_2$ solar cells, we have recently achieved η of more than 9.0% in heterojunction solar cells composed of a 20-nm-thick B-doped p-$BaSi_2$ layer on an n-Si substrate,[44,45] wherein the hole concentration p was set to 2×10^{18} cm^{-3}. This η is the highest ever reported for solar cells, fabricated using semiconducting silicides. The p-$BaSi_2$/n-Si heterojunction was chosen as a preliminary step toward the realization of a $BaSi_2$ homojunction solar cell because large conduction-band and valence-band offsets promote the separation of photogenerated carriers in both p-$BaSi_2$ and n-Si.[44] The contribution of carriers generated in the 20-nm-thick p-$BaSi_2$ layer to the overall photocurrent density was limited to be approximately 18%. To realize $BaSi_2$ thin-film solar cells, the contribution of $BaSi_2$ should be improved much further by increasing the thickness of the p-$BaSi_2$ layer. However, we do not have sufficient data to analyze the minority-carrier properties of B-doped p-$BaSi_2$.

In this work we performed minority-carrier lifetime τ measurement of B-doped p-$BaSi_2$ with various p values by microwave-detected photoconductivity decay (μ-PCD; KOBELCO LTA-1512EP) measurement. Furthermore, we also conducted photoresponse measurement to confirm the results of μ-PCD measurement.

2. Experimental methods

An ion-pumped molecular beam epitaxy (MBE; R-DEC) system equipped with a Knudsen cell (K-cell) for Ba and B, as well as an electron beam evaporation source for Si was used for sample preparation. The details of the growth procedure are described in Refs. 44 and 46. For τ measurements, we used a floating-zone (FZ) n-Si(111) substrate with resistivity $\rho >$ 1000 Ωcm. Briefly, a 5-nm-thick $BaSi_2$ epitaxial layer was grown by reactive deposition epitaxy, that is, Ba deposition on a hot n-Si(111) substrate at a substrate temperature of T_S = 500 °C, and it was used as a template. The template layer works as a seed crystal for the subsequent $BaSi_2$ layer. Next, Ba, Si, and B were coevaporated to form approximately 600-nm-thick *a*-axis-oriented B-doped p-$BaSi_2$ epitaxial films at T_S = 600 °C. The crucible temperature of the B K-cell (T_B) was varied (1000, 1100, and 1350 °C) to change p. Finally, samples were capped *in situ* with 2–3-nm-thick a-Si at T_S < 200 °C to passivate the $BaSi_2$

surface.[47,48] The electrical properties were analyzed at room temperature (RT) by Hall measurements using the van der Pauw method.

For photoresponse measurement, we used Czochralski (CZ) n^+-Si(111) with ρ < 0.009 Ωcm to eliminate the contribution of carriers generated in n^+-Si, and we grew 600-nm-thick *a*-axis-oriented B-doped p-$BaSi_2$ epitaxial films by setting T_B to 1000 or 1350 °C. For comparison, 600-nm-thick n-$BaSi_2$ layers were also formed. They were capped *in situ* with a-Si capping layers. The front contact was formed by sputtering 1-mm-diameter and 70-nm-thick ITO, and the rear contact was prepared using Al by sputtering. The crystallinity of $BaSi_2$ was investigated by reflection high-energy electron diffraction (RHEED) and θ-2θ X-ray diffraction (XRD; Rigaku Smart Lab) analyses with Cu *K*α radiation. Ge(220) single crystals were used to render X-rays monochromatic for measuring full width at half maximum (FWHM) values from an ω–scan X-ray rocking curve. τ was investigated from the excess-carrier recombination kinetics analyzed by the μ-PCD measurement. Excess carriers were generated by a 5 ns laser pulse with a wavelength of 349 nm, and photoconductivity decay was measured from the reflectivity of microwaves with a frequency of 26 GHz. The laser intensity was set to 1.3×10^5 W/cm^2. Photoresponse properties were evaluated at RT using a lock-in technique with a xenon lamp and a 25 cm focal-length single monochromator (Bunko Keiki; SM-1700A). The light intensity was calibrated with a pyroelectric sensor (Melles Griot; 13PEM001/J). All measurements were performed using a mask with 1-mm-diameter holes.

3. Results and discussion

3.1 Crystalline qualities

Figure 1 shows the θ-2θ XRD and RHEED patterns of p-$BaSi_2$ layers with different *p* values prepared for the μ-PCD measurement. The RHEED patterns were obtained along the Si[$11\bar{2}$] azimuth prior to the deposition of the a-Si layer. In the XRD patterns, we observed diffraction lines of only (100)-oriented $BaSi_2$ such as (200), (400), and (600). This shows

that the *a*-axis-oriented $BaSi_2$ was grown epitaxially for all the samples. No peak shift was observed in the three samples, as shown by broken lines in Fig. 1. Similar XRD and RHEED patterns were also observed for samples prepared for photoresponse measurement. The FWHM values obtained from an ω–scan X-ray rocking curve using a $BaSi_2$(600) diffraction peak were 0.47, 0.68, and 0.24 deg for samples grown at T_B = 1000, 1100, and 1350 °C, respectively. These values are larger than 0.2 deg obtained for undoped $BaSi_2$,[46] indicating that the crystalline quality of $BaSi_2$ is degraded by B doping. However, the FWHM does not increase monotonically with the B concentration.

The p values were measured to be 1.4×10^{16}, 9.0×10^{16}, and 3.9×10^{18} cm^{-3} for samples grown at T_B = 1000, 1100, and 1350 °C, respectively. Figure 2 shows the relationship between the measured p and the mobility μ_p of B-doped p-$BaSi_2$ layers. As p increased, μ_p decreased. This trend is usually predicted from ionized impurity scattering in conventional semiconductors.

3.2 Minority-carrier lifetime

Figure 3(a) shows the μ-PCD decay curves of B-doped p-$BaSi_2$ layers with different p. The reflectivity of the microwave is proportional to Δn. Thus, the time constant of the decay mode of excess carriers can be derived from a μ-PCD decay curve. The absorption coefficient at a wavelength λ of 349 nm is higher than 5×10^5 cm^{-1},[26] indicating that most of the photons are absorbed in the p-$BaSi_2$ layers. As the photon energy at λ = 349 nm is 3.55 eV, the area photon density was calculated to be $1.3\times10^5 \times 5\times10^{-9} / (1.6\times10^{-19} \times 3.55) \cong 1.1\times10^{15}$ cm^{-2}. Assuming that these photons are distributed over the 600-nm-thick p-$BaSi_2$ layers uniformly, the excess carrier density Δn was estimated to be approximately $1.1\times10^{15} / 0.6\times10^{-4} \cong 1.8\times10^{19}$ cm^{-3} on average. We chose Δn to be higher than the density of majority carriers (holes) for all the samples, to ensure that the carrier recombination mechanisms are the same among them. More than 95% of the incident light is absorbed within 50 nm from the surface. Because the electron concentration of the FZ n-Si substrate was lower than the hole concentration of p-$BaSi_2$, the depletion layer width was calculated to be less than 1 nm in the p-$BaSi_2$ layer from the Si/p-$BaSi_2$ interface. Hence, the effect of the built-in electric field inducing the charge separation of photogenerated electron-hole pairs, which therefore leads to the extension of the excess-carrier lifetime, can be neglected.

According to previous works,[49,50] the decay can be divided into three modes on the basis of the decay rate: Auger recombination and Shockley-Read-Hall (SRH) recombination without and with the carrier-trapping effect. The decay curve was fitted well using

$$I(t) = I_1 \exp(-\frac{t}{\tau_{\text{Auger}}}) + I_2 \exp(-\frac{t}{\tau_{\text{SRH}}}) + I_3 \exp(-\frac{t}{\tau_{\text{SRH-trapping}}}) . \quad (1)$$

Here, I_1, I_2, and I_3 are the coefficients, and τ_{Auger}, τ_{SRH}, and $\tau_{\text{SRH-trapping}}$ are the time constants for the three decay modes, respectively. The initial rapid decay is attributed to the Auger recombination process. Assuming that all the incoming photons are absorbed within the p-$BaSi_2$ layer, Δn is on average one to three orders of magnitude larger than the majority-carrier concentration at equilibrium in p-$BaSi_2$ (1.4×10^{16} – 3.9×10^{18} cm^{-3}). Therefore, the fast decay mode arising from the multicarrier recombination is inevitable at this high injection level. The decay, the region of which is marked by a black line in Fig. 3(a), is caused by the SRH recombination mechanism without the carrier-trapping effect. τ_{SRH} usually determines the minority-carrier lifetime, which should be sufficiently high to achieve a high η in solar cells. Therefore, in this work we use τ_{SRH} as a measure to characterize the minority-carrier lifetime of p-$BaSi_2$. The slow decay is attributed to SRH recombination with the carrier trapping effect, which is reportedly not dominant in $BaSi_2$.[49] A similar decay mechanism has also been reported for silicon.[51-53]

In Fig. 3(a), we see that the excess carriers decayed quickly in samples with a larger p, meaning that τ_{SRH} decreases with increasing p. From the decay curves, we then extracted τ_{SRH} for each sample using Eq. (1) and plotted it in Fig. 3(b) against p. τ decreased from approximately 2 μs to 0.5 and 0.07 μs as p increased from 1.4×10^{16} cm^{-3} to 9.0×10^{16} and 3.9×10^{18} cm^{-3}, respectively. The minority-carrier diffusion length L is proportional to the square root of τ. On the basis of these results, we therefore expect L for p-$BaSi_2$ with $p \sim 10^{16}$ cm^{-3} to be approximately 10 times larger than that with $p \sim 10^{18}$ cm^{-3}. As we can control p by controlling the B concentration, the increase in the B concentration is conceivably responsible for the decrease in τ through the generation of more recombination centers. The decrease in the carrier lifetime due to B through the formation of the B-O complex is observed in B-doped CZ-Si solar cells.[54,55] Since a recent study also revealed the existence of O inside $BaSi_2$ layers,[56] this hypothesis is probably reasonable to explain the degradation of τ. However, of course we should further investigate the cause of this τ degradation.

3.3 Photoresponse spectra

The linear current-voltage (*I-V*) characteristics were confirmed in all the samples such as in diodes with an n^+-$BaSi_2$/p^+-Si tunnel junction,[27,57] indicating that the p-$BaSi_2$/n^+-Si did not act as a rectifying diode. We are not sure why the rectifying properties disappear in the *I-V*

characteristics when we employ heavily doped n-Si substrates. This is different from the distinct rectifying *I-V* characteristics obtained in p-$BaSi_2$/n-Si diodes with a low *n*.[44,45)]

Figures 4(a) and 4(b) show the photoresponse properties of samples with $p = 1.4 \times 10^{16}$ cm^{-3} and $p = 3.9 \times 10^{18}$ cm^{-3}, respectively, at various reverse bias voltages (V_{bias}). V_{bias} was applied to p-$BaSi_2$ with respect to n-Si. Under this bias condition, the electric field in p-$BaSi_2$ and the large band offsets at the heterointerface promote the separation of photogenerated carriers. The photogenerated minority carriers (electrons) in p-$BaSi_2$ are transferred to n-Si and sensed as a current in the external circuit. On the other hand, the contribution of the photogenerated holes in n-Si was negligible owing to such a high impurity doping ($> 10^{19}$ cm^{-3}). $EQE = R \times \hbar\omega$, where R is the photoresponsivity and $\hbar\omega$ is the photon energy.[58)] Both Figs. 4(a) and 4(b) show that the photocurrent sharply increased at wavelengths (λ) shorter than 1000 nm, which corresponds to the optical absorption edge of $BaSi_2$. The *EQE* reached a maximum in the range of 600–800 nm. With increasing bias voltage, the *EQE* increased. This can be explained as follows. The *EQE* presented here is not the same as that usually characterized in a pn-junction solar cell under the short-circuit condition, namely, $V_{bias} = 0$ V, wherein photogenerated carriers are collected by diffusion. In the present work, however, the photogenerated minority carriers (electrons) in p-$BaSi_2$, where the electric field exists because of the bias voltage, are collected by drifting toward n-Si. The *EQE* is proportional to the ratio of the carrier lifetime to the carrier transit time.[58)] With increasing bias voltage, the drift velocity of carriers increases, leading to a decrease in the carrier transit time. Therefore, more electrons generated in p-$BaSi_2$ reach the n-Si region before recombination. This is why the *EQE* increases with V_{bias}. Considering that α for $BaSi_2$ exceeds 10^4 cm^{-1} at $\lambda = 800$ nm, it is reasonable to consider that almost all the photons at wavelengths shorter than 800 nm are absorbed within a 600-nm-thick p-$BaSi_2$ film. Thus, we can safely state that the contribution of photocurrent is mainly ascribed to p-$BaSi_2$. The *EQE* exceeded 80% at $\lambda = 800$ nm and $V_{bias} = -0.2$ V in the sample with a low *p* of 1.4×10^{16} cm^{-3}. In contrast, the *EQE* did not reach 60% even when V_{bias} was −3.0 V for the sample with a high *p* of 3.9×10^{18} cm^{-3}.

For comparison, we summarized the *EQE* spectra of these two samples in Fig. 5 together with a reference sample, that is, 600-nm-think n-$BaSi_2$. V_{bias} was set to −1.0 V. The *EQE* exceeds 100% for p-$BaSi_2$ with the low *p* of 1.4×10^{16} cm^{-3}. When the transit time becomes much shorter than the carrier lifetime, the *EQE* may exceed 100%. This phenomenon has been applied to practical devices such as photoconductors. On the basis of this result, we can state that B-doped p-$BaSi_2$ with a low *p* performs better than that with a

high p. The EQE of B-doped p-$BaSi_2$ with p=1.4 × 10^{16} cm^{-3} is about 10 times higher than that with p = 3.9 × 10^{18} cm^{-3} over the entire wavelength range. This result is consistent with the improvement of τ shown in Fig. 3(b). Photons with lower energies penetrate deeper into the $BaSi_2$ bulk region owing to the small α, and hence produce photoexcited carriers in the deeper region. On the other hand, photons with higher energies are absorbed in the region close to the surface. The longer τ becomes, the more photoexcited carriers are extracted to the external circuit before recombination. The EQE of p-$BaSi_2$ with p=1.4 × 10^{16} cm^{-3} is distinctly higher than that of n-$BaSi_2$, which shows excellent minority-carrier properties such as a long minority-carrier lifetime (τ ~ 10 μs)[49,50] and a large minority-carrier diffusion length (L ~ 10 μm).[32] The low-B-doped $BaSi_2$ shows better performance in terms of photoresponsivity than n-$BaSi_2$. Since minority-carrier types differ, we cannot directly compare minority-carrier transport properties. However, these results demonstrate the great potential of low-B-doped p-$BaSi_2$ as a novel absorption layer for solar cells.

4. Conclusions

600-nm-thick B-doped p-$BaSi_2$ films with p varied from 1.4 × 10^{16} to 3.9 × 10^{18} cm^{-3} were grown by MBE on (111)-oriented FZ n-Si substrates for μ-PCD measurement and on (111)-oriented CZ n^+-Si substrates for photoresponse measurement. The μ-PCD measurement revealed that τ_{SRH} for B-doped p-$BaSi_2$ depends significantly on p. τ_{SRH} increased from 0.07 to 2 μs as p decreased from 3.9 × 10^{18} to 1.4 × 10^{16} cm^{-3}. The improvement of τ_{SRH} was confirmed by photoresponse measurement. The EQE of the sample with p = 1.4 × 10^{16} cm^{-3} exceeded 80% at a reverse bias voltage of 0.2 V. This was approximately one order of magnitude higher than that with p = 3.9 × 10^{18} cm^{-3}, and is even higher than that of n-$BaSi_2$ with n on the order of 10^{16} cm^{-3}. On the basis of these results, we conclude that B-doped p-$BaSi_2$ with low p values is promising as an active layer in $BaSi_2$ solar cells.

Acknowledgments

This work was financially supported by the Japan Science and Technology Agency (JST/CREST) and by a Grant-in-Aid for Scientific Research A (15H02237) from the Japan Society for the Promotion of Science (JSPS). R.T. was financially supported by a Grant-in-Aid for JSPS Fellows (15J02139).

References

1) V. V. Tyag, N. A. A. Rahim, N. A. Rahi, and J. A. L. Selvaraj, Renewable and Sustainable Energy Rev. **20**, 443 (2013).
2) S. Fonash, *Solar Cell Device Physics* (Elsevier, Amsterdam, 2010) p. 95.
3) R. G. Gordon, J. Proscia, F. B. Ellis Jr., and A. E. Delahoy, Sol. Energy Mater. **18**, 263 (1989).
4) P. Campbell, Sol. Energy Mater. **21**, 165 (1990).
5) H. Sasaki, H. Morikawa, Y. Matsuno, M. Deguchi, T. Ishihara, H. Kumabe, T. Murotani, and S. Mitsui, Jpn. J. Appl. Phys. **33**, 3389 (1994).
6) J. Meier, S. Dubail, R. Platz, P. Torres, U. Kroll, J. A. A. Selvan, N. P. Vaucher, Ch. Hof, D. Fischer, H. Keppner, R. Fluckiger, A. Shah, V. Shklover, and K.-D. Ufert, Sol. Energy Mater. Sol. Cells **49**, 35 (1997).
7) O. Vetterl, F. Finger, R. Carius, P. Hapke, L. Houben, O. Kluth, A. Lambertz, A. Mück, B. Rech, and H. Wagner, Sol. Energy Mater. Sol. Cells **62**, 97 (2000).
8) A. Poruba, A. Fejfar, Z. Remes, J. Springer, M. Vanecek, and J. Kocka, J. Appl. Phys. **88**, 148 (2000).
9) J. Müller, B. Rech, J. Springer, and M. Vanecek, Sol. Energy **77**, 917 (2004).
10) M, Berginski, J. Hüpkes, M. Schulte, G. Schöpe, H. Stiebig, B. Rech, and M. Wuttig, J. Appl. Phys. **101**, 074903 (2007).
11) D. Zhou and R. Biswas, J. Appl. Phys. **103**, 093102 (2008).
12) A. Hongsingthong, T. Krajangsang, I. A. Yunaz, S. Miyajima, and M. Konagai, Appl. Phys. Express **3**, 051102 (2010).
13) H. Sai, Y. Kanamori, and M. Kondo, Appl. Phys. Lett. **98**, 113502 (2011).
14) H. Cui, P. R. Campbell, and M. A. Green, Energy Procedia **33**, 118 (2013).
15) D. W. Kang, J. Y. Kwon, J. Shim, H. M. Lee, and M. K. Han, Sol. Energy Mater. Sol. Cells **105**, 317 (2012).
16) K. Masuko, M. Shigematsu, T. Hashiguchi, D. Fujishima, M. Kai, N. Yoshimura, T. Yamaguchi, Y. Ichihashi, T. Mishima, N. Matsubara, T. Yamanishi, T. Takahama, M. Taguchi, E. Maruyama, and S. Okamoto, IEEE J. Photovoltaics **4,** 1433 (2014).
17) M. Taguchi, A. Yano, S. Tohoda, K. Matsuyama, Y. Nakamura, T. Nishiwaki, and E. Maruyama, IEEE J. Photovoltaics **4,** 96 (2014).
18) A. Romeo, A. Terheggen, D. Abou-Ras, D. L. Batzner, F. J. Haug, M. Kalin, D. Rudmann, and A. N. Tiwari, Prog. Photovoltaics **12**, 93 (2004).
19) I. Repins, M. A. Contreras, B. Egaas, C. DeHart, J. Scharf, C. L. Perkins, B. To, and R.

Noufi, Prog. Photovoltaics **16**, 235 (2008).
20) M. A. Green and S. R. Wenham, Appl. Phys. Lett. **65**, 2907 (1994).
21) H. Katagiri, K. Jimbo, W. S. Maw, K. Oishi, M. Yamazaki, H. Araki, and A. Takeuchi, Thin Solid Films **517**, 2455 (2009).
22) K. Tanaka, M. Oonuki, N. Moritake, and H. Uchiki, Sol. Energy Mater. Sol. Cells **93**, 583 (2009).
23) W. W. Yu, L. Qu, W. Guo, and X. Peng, Chem. Mater. **15**, 2854 (2003).
24) D. B. Migas, V. L. Shaposhnikov, and V. E. Borisenko, Phys. Status Solidi B **244**, 2611 (2007).
25) K. Morita, Y. Inomata, and T. Suemasu, Thin Solid Films **508**, 363 (2006).
26) K. Toh, T. Saito, and T. Suemasu, Jpn. J. Appl. Phys. **50**, 068001 (2011).
27) W. Du, M. Suzuno, M. Ajmal Khan, K. Toh, M. Baba, K. Nakamura, K. Toko, N. Usami, and T. Suemasu, Appl. Phys. Lett. **100**, 152114 (2012).
28) S. Koike, K. Toh, M. Baba, K. Toko, K. O. Hara, N. Usami, N. Saito, N. Yoshizawa, and T. Suemasu, J. Cryst. Growth **378**, 198 (2013).
29) W. Du, R. Takabe, M. Baba, H. Takeuchi, K. O. Hara, K. Toko, N. Usami, and T. Suemasu, Appl. Phys. Lett. **106**, 122104 (2015).
30) M. Kumar, N. Umezawa, and M. Imai, Appl. Phys. Express **7**, 071203 (2014).
31) M. Kumar, N. Umezawa, and M. Imai, J. Appl. Phys. **115**, 203718 (2014).
32) M. Baba, K. Toh, K. Toko, N. Saito, N. Yoshizawa, K. Jiptner, T. Sakiguchi, K. O. Hara, N. Usami, and T. Suemasu, J. Cryst. Growth **348**, 75 (2012).
33) M. Kumar, N. Umezawa, and M. Imai, Ext. Abstr. 63rd Japan Society of Applied Physics Spring Meeti., 2016, 21a-S223-2.
34) T. Suemasu, Jpn. J. Appl. Phys. **54**, 07JA01 (2015).
35) M. Kobayashi, Y. Matsumoto, Y. Ichikawa, D. Tsukada, and T. Suemasu, Appl. Phys. Express **1**, 051403 (2008).
36) M. Takeishi, Y. Matsumoto, R. Sasaki, T. Saito, and T. Suemasu, Phys. Procedia **11**, 27 (2011).
37) M. Ajmal Khan, T. Saito, K. Nakamura, M. Baba, W. Du, K. Toh, K. Toko, and T. Suemasu, Thin Solid Films **522**, 95 (2012).
38) M. Ajmal Khan, K. O. Hara, W. Du, M. Baba, K. Nakamura, M. Suzuno, K. Toko, N. Usami, and T. Suemasu, Appl. Phys. Lett. **102** 112107 (2013).
39) M. Ajmal Khan, K. Nakamura, W. Du, K. Toko, N. Usami, and T. Suemasu, Appl. Phys. Lett. **104**, 252104 (2014).

40) R. Takabe, M. Baba, K. Nakamura, W. Du, M. A. Khan, S. Koike, K. Toko, K. O. Hara, N. Usami, and T. Suemasu, Phys. Status Solidi C **10,** 1753 (2013).
41) K. O. Hara, Y. Hoshi, N. Usami, Y. Shiraki, K. Nakamura, K. Toko, and T. Suemasu, Thin Solid Films **557,** 90 (2014).
42) K. O. Hara, Y. Hoshi, N. Usami, Y. Shiraki, K. Nakamura, K. Toko, and T. Suemasu, Thin Solid Films **534**, 470 (2013).
43) K. O. Hara, N. Usami, Y. Hoshi, Y. Shiraki, M. Suzuno, K. Toko, and T. Suemasu, Jpn. J. Appl. Phys. **50**, 121202 (2011).
44) D. Tsukahara, S. Yachi, H. Takeuchi, R. Takabe, W. Du, M. Baba, Y. Li, K. Toko, N. Usami, and T. Suemasu, Appl. Phys. Lett. **108**, 152101 (2016).
45) S. Yachi, R. Takabe, H. Takeuchi, K. Toko, and T. Suemasu, Appl. Phys. Lett. **109**, 072103 (2016).
46) R. Takabe, K. Nakamura, M. Baba, W. Du, M. A. Khan, K. Toko, M. Sasase, K. O. Hara, N. Usami, and T. Suemasu, Jpn. J. Appl. Phys. **53**, 04ER04 (2014).
47) R. Takabe, K. O. Hara, M. Baba, W. Du, N. Shimada, K. Toko, N. Usami, and T. Suemasu, J. Appl. Phys. **115**, 193510 (2014).
48) R. Takabe, H. Takeuchi, W. Du, K. Ito, K. Toko, S. Ueda, A. Kimura, and T. Suemasu, J. Appl. Phys. **119**, 165304 (2016).
49) K. O. Hara, N. Usami, K. Toh, M. Baba, K. Toko, and T. Suemasu, J. Appl. Phys. **112**, 083108 (2012).
50) K. O. Hara, N. Usami, K. Nakamura, R. Takabe, M. Baba, K. Toko, and T. Suemasu, Appl. Phys. Express **6**, 112302 (2013).
51) J. A. Hornbeck and J. R. Haynes, Phys. Rev. **97**, 311 (1955).
52) D. Macdonald and A. Cuevas, Appl. Phys. Lett. **74**, 1710 (1999).
53) Y. Hu, H. Schøn, Ø. Nielsen, E. Johannes Øvrelid, and L. Arnberg, J. Appl. Phys. **111**, 053101 (2012).
54) S. W. Glunz, S. Rein, W. Warta, J. Knobloch, and W. Wettling, Sol. Energy Mater. Sol. Cells **65,** 219 (2001).
55) S. W. Glunz, S. Rein, J. Y. Lee, and W. Warta, J. Appl. Phys. **90**, 2397 (2001).
56) W. Du, R. Takabe, H. Takeuchi, D. Tsukahara, M. Baba, K. Toko, and T. Suemasu, submitted to Thin Solid Films.
57) T. Saito, Y. Matsumoto, M. Suzuno, M. Takeishi, R. Sasaki, T. Suemasu, and N. Usami, Appl. Phys. Express **3**, 021301 (2010).–
58) S. M. Sze, *Physics of Semiconductor Devices* (Wiley, New York, 1981) 2nd ed., p. 744.

Figure Captions

Fig. 1. θ-2θ XRD and RHEED patterns observed along the Si[$11\bar{2}$] azimuth of p-$BaSi_2$ layers with various p. The RHEED pattern was observed immediately after the growth of p-$BaSi_2$. The asterisk (*) indicates the peak for the Si substrate used. Broken lines are a guide to the eyes.

Fig. 2. Relationship between measured hole concentration and mobility of B-doped p-$BaSi_2$.

Fig. 3. (a) Photoconductivity decay curves of B-doped $BaSi_2$ with different p. Black lines indicate the regions of decay driven by the SRH recombination mechanism. (b) Dependence of τ_{SRH} on hole concentration.

Fig. 4. *EQE* spectra of B-doped p-$BaSi_2$ with (a) $p = 1.4 \times 10^{16}$ cm^{-3} and (b) $p = 3.9 \times 10^{18}$ cm^{-3} at various reverse bias voltages (V_{bias}) applied between the top and bottom electrodes.

Fig. 5. *EQE* spectra of B-doped p-$BaSi_2$ with $p = 1.4 \times 10^{16}$ cm^{-3} and $p = 3.9 \times 10^{18}$ cm^{-3}, and intrinsic n-$BaSi_2$ ($n \sim 10^{16}$ cm^{-3}) at $V_{bias} = -1.0$ V applied between the top and bottom electrodes.

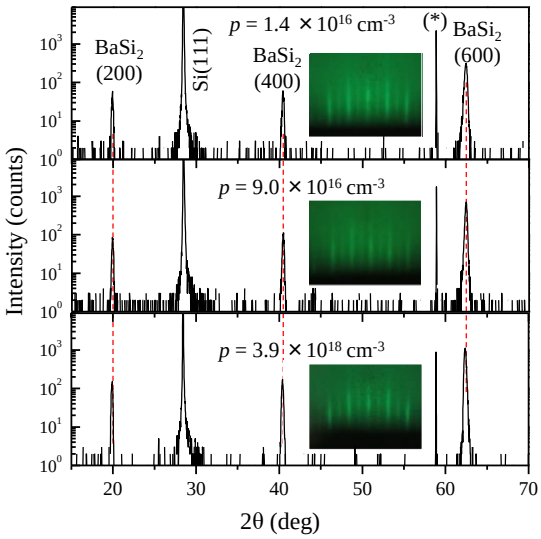
Intensity (counts)
2θ (deg)
BaSi2 (200)
Si(111)
BaSi2 (400)
(*)
BaSi2 (600)
p = 1.4 × 10^16 cm^-3
p = 9.0 × 10^16 cm^-3
p = 3.9 × 10^18 cm^-3

Fig. 1

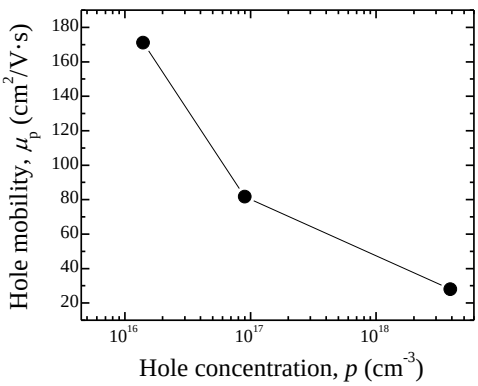
Hole mobility, μ_p ($cm^2/V \cdot s$)
180
160
140
120
100
80
60
40
20
10^{16}
10^{17}
10^{18}
Hole concentration, p (cm^{-3})

Fig. 2

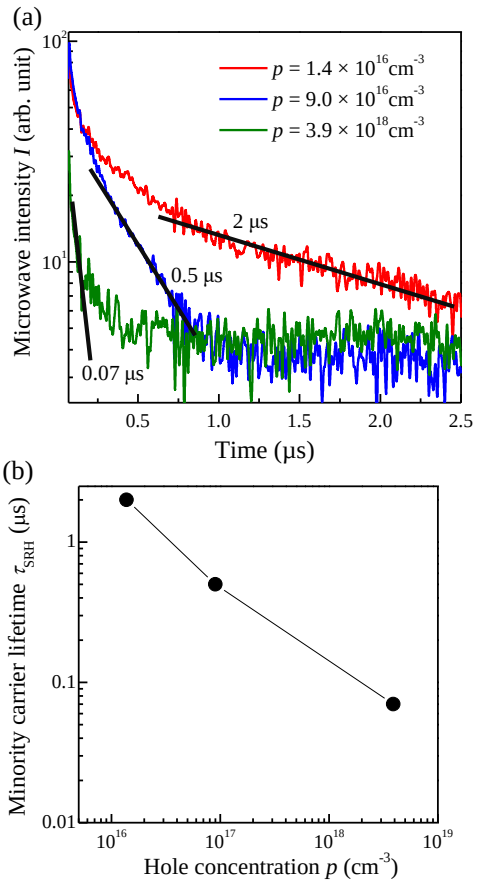
(a)
Microwave intensity I (arb. unit)
Time (μs)
p = 1.4 × 10^16 cm^-3
p = 9.0 × 10^16 cm^-3
p = 3.9 × 10^18 cm^-3
2 μs
0.5 μs
0.07 μs
(b)
Minority carrier lifetime τ_SRH (μs)
Hole concentration p (cm^-3)

Fig. 3

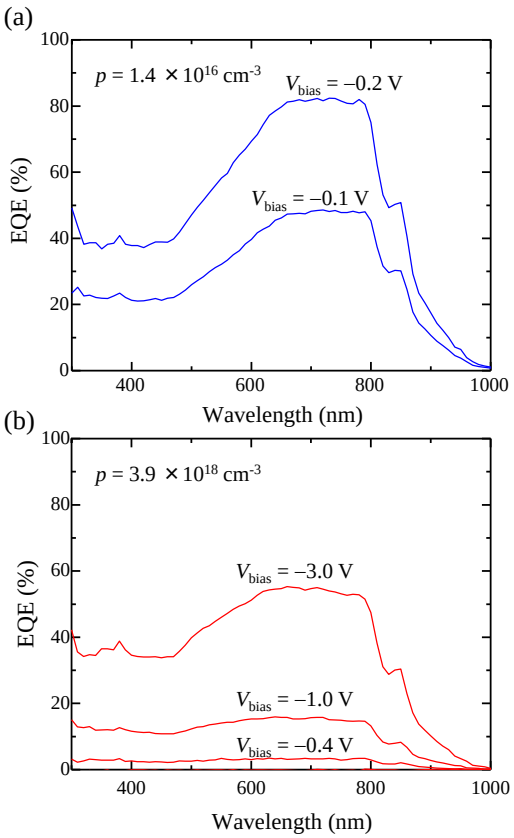
(a)
p = 1.4 × 10^16 cm^-3
V_bias = –0.2 V
V_bias = –0.1 V
EQE (%)
Wavelength (nm)
(b)
p = 3.9 × 10^18 cm^-3
V_bias = –3.0 V
V_bias = –1.0 V
V_bias = –0.4 V
EQE (%)
Wavelength (nm)

Fig. 4

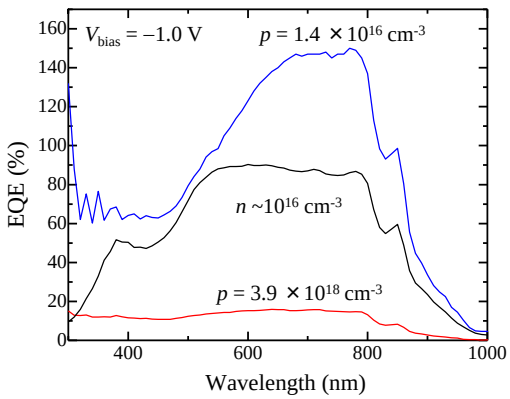
V_{bias} = –1.0 V
p = 1.4 × 10^{16} cm^{-3}
n ~10^{16} cm^{-3}
p = 3.9 × 10^{18} cm^{-3}
EQE (%)
Wavelength (nm)
0
20
40
60
80
100
120
140
160
400
600
800
1000

Fig. 5